



# Thermodynamic control of quantum defects on single-walled carbon nanotubes†

Cite this: *Chem. Commun.*, 2019, 55, 13757

Received 20th July 2019,  
Accepted 21st October 2019

DOI: 10.1039/c9cc05623h

rsc.li/chemcomm

Yutaka Maeda,<sup>a</sup> Hiyori Murakoshi,<sup>a</sup> Haruto Tambo,<sup>a</sup> Pei Zhao,<sup>b</sup> Kiyonori Kuroda,<sup>a</sup> Michio Yamada,<sup>a</sup> Xiang Zhao,<sup>c</sup> Shigeru Nagase<sup>d</sup> and Masahiro Ehara<sup>a,b</sup>

**Single-walled carbon nanotubes with designed quantum defects are prepared and characterized. The photoluminescence (PL) of the nanotubes can be modified by thermal treatment from 1215–1224 to 1249–1268 nm. Theoretical calculations suggest that the change in the PL spectra by thermal treatment can be explained by isomerization from kinetic to thermodynamic products.**

Single-walled carbon nanotubes (SWNTs) have attracted attention due to their remarkable mechanical stability and optoelectronic properties.<sup>1,2</sup> The ability to tailor the electronic properties of SWNTs based on their diameter and helicity makes them attractive materials as building blocks of electronic and optical nanodevices. Their suitability for an application depends on their band gap along with their absorption and photoluminescence (PL) properties which are observed in the near-infrared (NIR) region.<sup>3</sup> As NIR photoluminescent materials, SWNTs have been used in bio-imaging, telecommunications, and sensor design applications.<sup>4–8</sup> It has been reported that functionalization of SWNTs can control their NIR PL properties, resulting in the emergence of red-shifted PL peaks with high quantum yields.<sup>9–18</sup> Recent theoretical studies on functionalized SWNTs using density functional theory (DFT) revealed that the PL wavelength of functionalized SWNTs strongly depends on the addition patterns of addenda.<sup>19,20</sup> For example, the reaction of (6,5) SWNTs with phenyl diazonium salt afforded a new PL peak at 1119 nm. The theoretical calculation of these model compounds (hydrophenylated SWNTs) showed that the band gap energies depend on the addition patterns with the most

stable isomer being an *ortho* L<sub>-33</sub> adduct among their possible 1,2- and 1,4-addition isomers.<sup>20</sup> Conversely, the reaction of (6,5) SWNTs with 1,3-dibromopropane presented a new PL peak at 1215 nm.<sup>21</sup> The theoretical calculation of these model compounds, SWNT-(C<sub>3</sub>H<sub>6</sub>), showed that an *ortho* L<sub>-33</sub> adduct is the most stable isomer among the possible 1,2-addition isomers. Referring to the assignment of hydrophenylated SWNTs reported by Htoon and co-workers,<sup>20</sup> functionalized SWNTs with dibromopropane may not be the thermodynamic product.<sup>21</sup> Positional isomerization of fullerene derivatives has been studied to control their optical and electronic properties by changing the π electron system.<sup>22–24</sup> Encouraged by these reports on isomerization of fullerene derivatives, the thermodynamic control of the PL wavelength as well as the intensity of quantum defects on SWNTs is studied and the results are presented in this paper.

A series of functionalized SWNTs (**3a–3e** and **4a–4c**), depicted in Scheme 1, were designed and prepared by the reductive alkylation of SWNTs with dibromopropane (**1a–1e**) and dibromobutane derivatives (**2a–2c**), respectively. It has been reported that cycloaddition products of fullerenes are preferred for isomerization *via* a bond cleavage and recombination mechanism between fullerenes and addenda.<sup>25</sup> Recently, it has been reported that **1a** and **2a** are suitable reagents to afford cycloaddition products of SWNTs<sup>21</sup> similar to functionalization of fullerenes.<sup>26</sup> In addition, the bulkiness of addenda and the stability of the fragments after elimination strongly influenced the elimination reactions of functionalized SWNTs.<sup>27</sup> Thus, cyclic addenda having methyl or phenyl groups

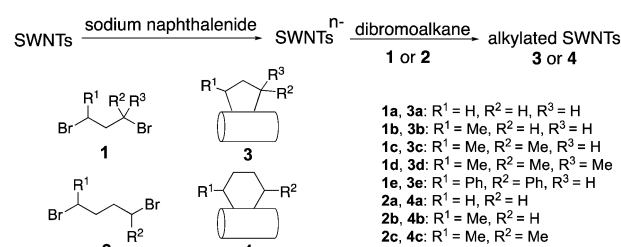
<sup>a</sup> Department of Chemistry, Tokyo Gakuji University, Tokyo 184-8501, Japan. E-mail: ymaeda@u-gakugei.ac.jp

<sup>b</sup> Research Center for Computational Science, Institute for Molecular Science, Okazaki, 444-8585, Japan. E-mail: ehara@ims.ac.jp

<sup>c</sup> Institute for Chemical Physics & Department of Chemistry, School of Science, State Key Laboratory of Electrical Insulation and Power Equipment, Xi'an Jiaotong University, Xi'an 710049, China

<sup>d</sup> Fukui Institute for Fundamental Chemistry (FIFC), Kyoto University, Sakyou-ku, Kyoto 606-8103, Japan

† Electronic supplementary information (ESI) available. See DOI: 10.1039/c9cc05623h



Scheme 1 Reductive alkylation of SWNTs.

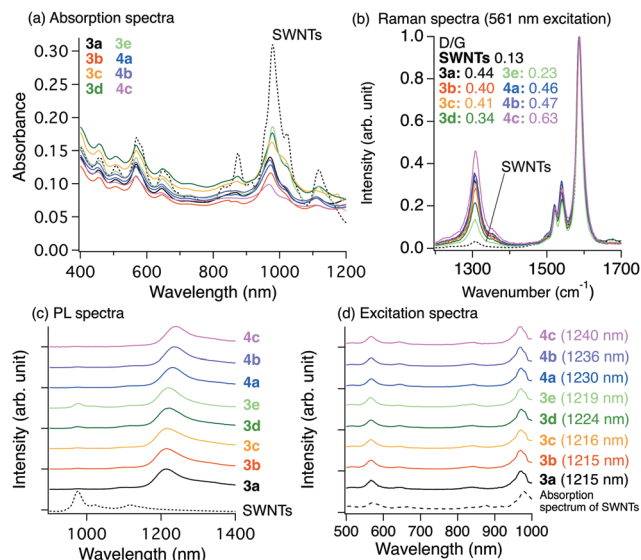


Fig. 1 (a) Absorption, (b) Raman (561 nm excitation), (c) PL (567 nm excitation), and (d) excitation spectra of SWNTs (the dotted line) and functionalized SWNTs (the solid line).

on SWNTs were synthesized for isomerization experiments. Fig. 1 shows the absorption, Raman, PL, and excitation spectra of **3** and **4**. The pristine (6,5) SWNTs show a PL peak at 980 nm at an excitation wavelength of 567 nm, which is assigned to the  $E_{11}$  PL of (6,5) SWNTs. After the functionalization, new red-shifted PL peaks were observed as dominant peaks (**3a**: 1215 nm,<sup>21</sup> **3b**: 1215 nm, **3c**: 1216 nm, **3d**: 1224 nm, **3e**: 1219 nm, **4a**: 1230 nm,<sup>21</sup> **4b**: 1236 nm, and **4c**: 1240 nm). The excitation spectra of these red-shifted PL peaks showed characteristic peaks at approximately 567 and 980 nm, which is in good agreement with the characteristic absorption peaks of (6,5) SWNTs, suggesting that these PL peaks originated from functionalized (6,5) SWNTs. As described above, it has been proposed that the PL wavelength of functionalized SWNTs depends on the addition patterns of addenda,<sup>19,20</sup> therefore, the selective emergence of a new red-shifted PL peak in functionalized (6,5) SWNTs indicates the high regioselectivity of (6,5) SWNTs in the reaction. In addition to the difference in the alkyl chain length between **3** and **4**, the substituents ( $R^1$ ,  $R^2$ , and  $R^3$ ) in **3d**, **3e**, **4b**, and **4c** affected the red-shifted PL wavelength. The difference in the PL wavelength between **3a** and **4a** can be caused by local strain induced by the addenda; this conclusion is based on the results of theoretical calculations that have been reported previously.<sup>21</sup>

Thermal treatment of the functionalized SWNTs was conducted at a heating rate of  $10\text{ }^\circ\text{C min}^{-1}$  under an atmosphere of nitrogen. The change in the functionalization degree of **3** and **4** was estimated from the relative  $E_{11}$  absorption peak intensities normalized at the local minimum ( $\sim 775\text{ nm}$ ) and the ratios of the D band toward the G band (D/G) in the Raman spectra (Fig. S1–S10, ESI<sup>†</sup>). An increase in the relative  $E_{11}$  absorption peak intensities and a decrease in the D/G ratio were observed as the temperature of thermal treatment increased (Fig. S11, ESI<sup>†</sup>). Results showed that **3a** and **4a** were more stable than **3b–3e** and **4b–4c**, respectively. These results indicate that the methyl and phenyl groups in the cyclic addenda promote the elimination of the addenda. The PL spectra of **3a–e** and **4a–c**

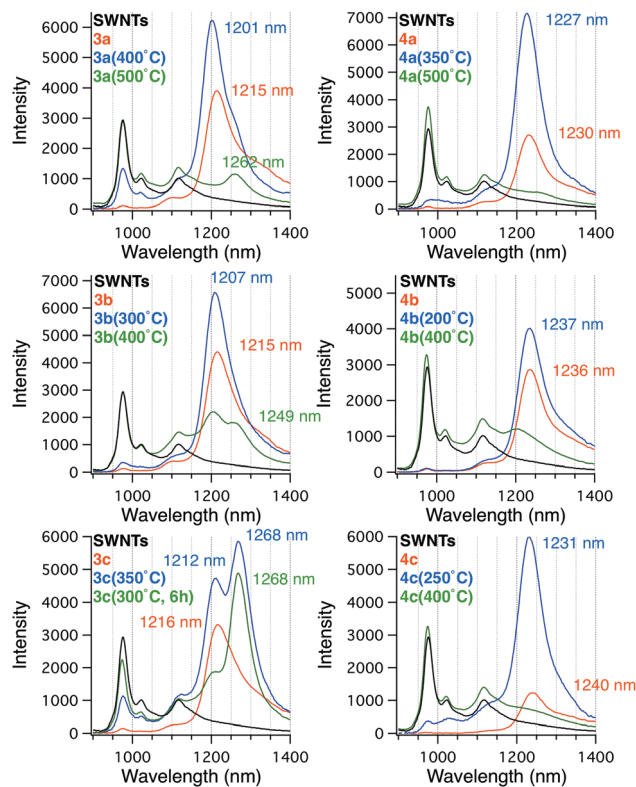


Fig. 2 PL spectra (567 nm excitation) of the functionalized SWNTs (**3a–3c** and **4a–4c**) before and after thermal treatment.

after thermal treatment can be observed in Fig. 2 and Fig. S12–S16 (ESI<sup>†</sup>). The red-shifted PL peak intensities of **3a–3c** and **4a–4c** increased with a decrease in the functionalization degree upon thermal treatment. Minor peak shifts in the red-shifted PL were observed and accompanied by an increase in the peak intensity after thermal treatment (**3a** (400  $^\circ\text{C}$ ): 1201 nm, **3b** (300  $^\circ\text{C}$ ): 1207 nm, **3c** (350  $^\circ\text{C}$ ): 1212 nm, **3d** (200  $^\circ\text{C}$ ): 1222 nm, **3e** (200  $^\circ\text{C}$ ): 1219 nm, **4a** (350  $^\circ\text{C}$ ): 1227 nm, **4b** (200  $^\circ\text{C}$ ): 1237 nm, and **4c** (250  $^\circ\text{C}$ ): 1231 nm). Similar blue shifts of PL peaks were also observed after thermal treatment of acyclic alkylated SWNTs, reported previously.<sup>27</sup> Interestingly, new PL peaks were observed from **3a–3d** at 1249–1268 nm after thermal treatment (**3a** (500  $^\circ\text{C}$ ): 1262 nm, **3b** (300  $^\circ\text{C}$ ): 1249 nm, **3c** (350  $^\circ\text{C}$ ): 1268 nm, and **3d** (300  $^\circ\text{C}$ ): 1242 nm (200  $^\circ\text{C}$ )). Notably, highly selective emergence of the PL peak at 1268 nm was achieved in **3c** by thermal treatment at 300  $^\circ\text{C}$  for 6 h. The good agreement of the excitation spectrum (1268 nm) of **3c** (300  $^\circ\text{C}$ , 6 h) with the absorption spectrum of (6,5) SWNTs suggests that the PL originates from the functionalized (6,5) SWNTs (Fig. S17, ESI<sup>†</sup>). After thermal treatment of **3e**, **4a**, **4b**, and **4c**, new PL peaks at longer wavelength are not observed. The emergence of new PL peaks at longer wavelengths in **3c** and **3d** at a relatively low temperature suggests that the thermal control of the PL wavelength involves a bond cleavage and a recombination process causing isomerization of the addenda. In the case of **3e**, it is believed that the elimination reaction proceeded preferentially as the thermal stability of **3e** is too low. In radical cyclization reactions of alkenyl radicals, it is known that the six-membered ring formation yield is lower than the five-membered ring formation yield.<sup>28</sup> This might be one of

the reasons for the elimination reactions of **4a** to **4c** to proceed preferentially over isomerization. In a previous report, the emergence of the corresponding red-shifted PL peak had not been observed from acyclic alkylated SWNTs after thermal treatment.<sup>13,27</sup>

Determining the local structures of functionalized SWNTs is necessary to reveal the origin of PL changes. However, as it is difficult to determine the local structure of functionalized SWNTs experimentally, DFT and time-dependent DFT calculations of model compounds are performed (Fig. 3 and Fig. S20, ESI†).<sup>29–32</sup> As mentioned above, the possibility of cycloaddition of SWNTs using **3a** and **4a** has been reported.<sup>21</sup> Therefore, we considered three model structures of the corresponding 1,2-cycloadducts. These isomers are distinguished by their abbreviations reported by Htoon and co-workers (Fig. 4).<sup>20</sup> It was reported that the calculated emission energies showed a similar tendency to the calculated absorption energies.<sup>33</sup> Therefore, instead of emission energies, absorption energies of the model compounds were calculated to decrease the computational cost of geometry optimization. In the present study, it is confirmed that absorption and emission trends of regioisomers of SWNT-(C<sub>3</sub>H<sub>6</sub>) calculated by CAM-B3LYP/STO-3G were the same (Table S2, ESI†). The relative energy, absorption wavelength, and C–C bond length between SWNTs and the substituents of the model compounds for **3a–3c** and **4a–4c** are shown in Fig. 5, Tables S3 and S4 (ESI†), respectively. Relative energies were also examined using the functionals with dispersion corrections; the effects of which are minor in the present system as shown in Table S8 (ESI†). The increase in the C–C bond length with an increase in the number of methyl substituents indicates the presence of steric repulsion between the methyl group and SWNTs. This result is consistent with the experimental results showing that the presence of methyl groups facilitates the elimination of addenda. In comparisons with model compounds with the same

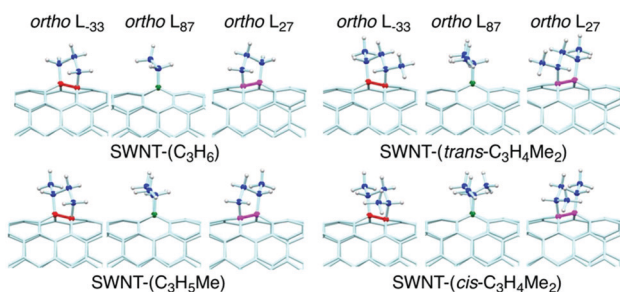


Fig. 3 Partial view of the optimized structures of functionalized (6,5) SWNTs by B3LYP/6-31G\*.

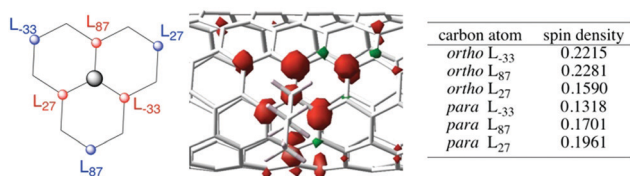


Fig. 4 Addition sites of functionalized SWNTs and the spin density of the <sup>n</sup>Bu-SWNT radical by UB3LYP/3-21G using 3-unit cells. The optimized structure is shown in Fig. S23 (ESI†).

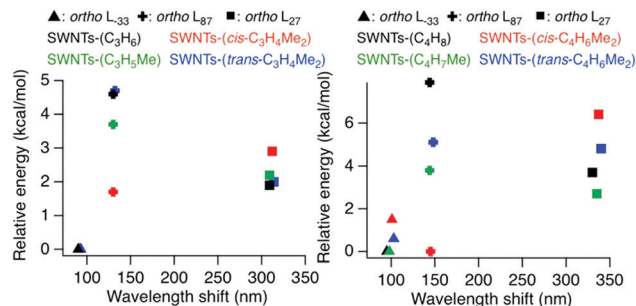


Fig. 5 Relative energies using DFT with B3LYP/6-31G\* and the calculated absorption wavelength shift from SWNTs of functionalized SWNTs using TD-DFT with B3LYP/3-21G.

addition patterns, the calculated absorption wavelength showed good agreement with the experimental PL wavelengths of **3a–3c** and **4a–4c**. The wavelengths of the 5-membered cyclic adducts are shorter than those of the 6-membered cyclic adducts in the same addition patterns, indicating that the calculated absorption wavelength is strongly dominated by the alkyl chain length and its addition patterns (*ortho* L<sub>-33</sub>: 880–893 nm, *ortho* L<sub>-87</sub>: 920–938 nm, and *ortho* L<sub>-27</sub>: 1099–1130 nm).<sup>20,33</sup> In addition, the results show that the substituted methyl groups influence the absorption wavelength of these cyclic addition products. The *ortho* L<sub>-33</sub> isomers are the most stable regardless of the addenda, suggesting that the *ortho* L<sub>-33</sub> isomers are not the potential compounds for the products before and after thermal treatment; this is because they have the highest relative stability and the shortest absorption wavelength.

In order to improve our understanding of candidate isomers for functionalized SWNTs before thermal treatment, the spin density of the *n*-butylated (6,5) SWNT (<sup>n</sup>Bu-SWNT) radical as a corresponding intermediate in the reductive alkylation is calculated. Results show that the carbon atom at the *ortho* L<sub>-87</sub> position has the highest spin density (Fig. 4, Fig. S23 and Table S5, ESI†). Therefore, *ortho* L<sub>-87</sub> isomers are potential compounds for kinetic products in the cyclization reaction. *ortho* L<sub>-27</sub> isomers have the potential as thermodynamic products after thermal treatment for **3**; this is because the *ortho* L<sub>-27</sub> isomers are more stable than the *ortho* L<sub>-87</sub> isomers, except for SWNT-(*cis*-C<sub>3</sub>H<sub>6</sub>Me<sub>2</sub>), and possess longer absorption wavelengths than the *ortho* L<sub>-87</sub> isomers. Htoon *et al.* reported the correction of the emission energy of functionalized SWNTs at an infinite length  $E_{11}^*(\infty)$  by DFT calculations using finite-length tube models.<sup>34</sup> Thus, corrections of the emission energies of SWNT-(C<sub>3</sub>H<sub>6</sub>) and SWNT-(*cis*-C<sub>3</sub>H<sub>4</sub>Me<sub>2</sub>) were conducted using the 3-unit model and using the following equation, which was proposed by Htoon and co-workers:<sup>34</sup>

$$E_{11}^*(\infty) = -0.59(E_{11} - E_{11}^*) + 1.25$$

where  $E_{11}$  and  $E_{11}^*$  represent the emission energies of the pristine SWNT and each functionalized SWNT, respectively. The corrected emission energies of functionalized SWNTs originating from *ortho* L<sub>-87</sub> and *ortho* L<sub>-27</sub> (Table 1) showed good agreement with the experimental values (**3a**: 1.03 eV, **3c**: 1.02 eV, **3a**(500 °C): 0.983 eV, and **3c**(300 °C, 6 h): 0.978 eV), strongly

**Table 1** Calculated emission energies for SWNT-(C<sub>3</sub>H<sub>6</sub>) and SWNT-(*trans*-C<sub>3</sub>H<sub>4</sub>Me<sub>2</sub>) after the correction

	Addition site	Calculated	
		$E_{11}^*(\infty)^a$ (eV)	$F^b$
SWNT-(C <sub>3</sub> H <sub>6</sub> )	<i>ortho</i> L <sub>-33</sub>	1.126	0.786
	<i>ortho</i> L <sub>87</sub>	1.075	0.881
	<i>ortho</i> L <sub>27</sub>	0.929	1.04
SWNT-( <i>trans</i> -C <sub>3</sub> H <sub>4</sub> Me <sub>2</sub> )	<i>ortho</i> L <sub>-33</sub>	1.125	0.759
	<i>ortho</i> L <sub>87</sub>	1.075	0.869
	<i>ortho</i> L <sub>27</sub>	0.929	1.032

<sup>a</sup> Calculated using the method of ref. 34. <sup>b</sup> Oscillator strength values are obtained using the 1-unit cell at the B3LYP/3-21G level of theory.

supporting the assignment of the local structure before and after thermal treatment of **3**. However, for clarification of the exact structure of functionalized SWNTs further studies are required.

In conclusion, control of the PL wavelength of quantum defects on SWNTs was achieved by thermal treatment. The combination of optical measurements and theoretical calculations is effective for understanding the structure and properties of SWNTs, including the isomerization of functionalized SWNTs. After thermal treatment, red-shifted PL observed from **3a–3d** at 1215–1219 nm decreased with an emergence of new PL peaks at 1249–1268 nm. Although the PL peak intensity was tuned, new PL peaks at longer wavelength were not observed from **3e**, **4a–4c**, and acyclic alkylated SWNTs after thermal treatment. The DFT and TD-DFT calculations showed that the absorption and emission energies of functionalized SWNTs are strongly dependent on the addition patterns. By demonstrating the relationship between the stability and the local band gap energy of the functionalized SWNT isomers, it can be seen that thermal isomerization from kinetic to thermodynamic products is one plausible explanation for the changes in the red-shifted PL wavelength of functionalized SWNTs.

This work was supported by JSPS KAKENHI Grant-in-Aid for Scientific Research (B) (17H02735, 16H06511, and 16H04104) and by the National Natural Science Foundation of China (Grant 21573172 and 21773181). The authors also acknowledge financial support from the PhD short-term academic visiting program and the Nanotechnology Platform Program (Molecule and Materials Synthesis: 20191102) of the Ministry of Education, Culture, Sports, Science, and Technology of Japan.

## Conflicts of interest

There are no conflicts to declare.

## Notes and references

- 1 S. Iijima and T. Ichihashi, *Nature*, 1993, **363**, 603–605.
- 2 D. S. Bethune, C. H. Klang, M. S. De Vries, G. Gorman, R. Savoy, J. Vazquez and R. Beyers, *Nature*, 1993, **363**, 605–607.
- 3 S. M. Bachilo, M. S. Strano, C. Kittrell, R. H. Hauge, R. E. Smalley and R. B. Weisman, *Science*, 2002, **298**, 2361–2366.
- 4 A. Högele, C. Galland, M. Winger and A. Imamoğlu, *Phys. Rev. Lett.*, 2008, **100**, 217401.
- 5 Z. Liu, S. Tabakman, K. Welsher and H. Dai, *Nano Res.*, 2009, **2**, 85–120.
- 6 K. Welsher, Z. Liu, S. P. Sherlock, J. T. Robinson, Z. Chen, D. Daranciang and H. Dai, *Nat. Nanotechnol.*, 2009, **4**, 773–780.
- 7 T. Endo, J. Ishi-Hayase and H. Maki, *Appl. Phys. Lett.*, 2015, **106**, 113106.
- 8 X. Ma, N. F. Hartmann, J. K. S. Baldwin, S. K. Doorn and H. Htoon, *Nat. Nanotechnol.*, 2015, **10**, 671–675.
- 9 S. Ghosh, S. M. Bachilo, R. A. Simonette, K. M. Beckingham and R. B. Weisman, *Science*, 2010, **330**, 1656–1659.
- 10 Y. Miyauchi, M. Iwamura, S. Mouri, T. Kawazoe, M. Ohtsu and K. Matsuda, *Nat. Photonics*, 2013, **7**, 715–719.
- 11 Y. Maeda, J. Higo, Y. Amagai, J. Matsui, K. Ohkubo, Y. Yoshigoe, M. Hashimoto, K. Eguchi, M. Yamada, T. Hasegawa, Y. Sato, J. Zhou, J. Lu, T. Miyashita, S. Fukuzumi, T. Murakami, K. Tohji, S. Nagase and T. Akasaka, *J. Am. Chem. Soc.*, 2013, **135**, 6356–6362.
- 12 Y. Piao, B. Meany, L. R. Powell, N. Valley, H. Kwon, G. C. Schatz and Y. Wang, *Nat. Chem.*, 2013, **5**, 840–845.
- 13 Y. Maeda, Y. Takehana, M. Yamada, M. Suzuki and T. Murakami, *Chem. Commun.*, 2015, **51**, 13462–13465.
- 14 Y. Maeda, E. Sone, A. Nishino, Y. Amagai, W. W. Wang, M. Yamada, M. Suzuki, J. Matsui, M. Mitsuishi, T. Okazaki and S. Nagase, *Chem. – Eur. J.*, 2016, **22**, 15373–15379.
- 15 Y. Maeda, S. Minami, Y. Takehana, J. S. Dang, S. Aota, K. Matsuda, Y. Miyauchi, M. Yamada, M. Suzuki, R. S. Zhao, X. Zhao and S. Nagase, *Nanoscale*, 2016, **8**, 16916–16921.
- 16 H. Kwon, A. Furmanchuk, M. Kim, B. Meany, Y. Guo, G. C. Schatz and Y. Wang, *J. Am. Chem. Soc.*, 2016, **138**, 6878–6885.
- 17 T. Shiraki, T. Shiraiishi, G. Juhász and N. Nakashima, *Sci. Rep.*, 2016, **6**, 28393.
- 18 A. H. Brozena, M. Kim, L. R. Powell and Y. Wang, *Nat. Rev. Chem.*, 2019, **3**, 375–392.
- 19 S. Kilina, J. Ramirez and S. Tretiak, *Nano Lett.*, 2012, **12**, 2306–2312.
- 20 X. He, B. J. Gifford, N. F. Hartmann, R. Ihly, X. Ma, S. V. Kilina, Y. Luo, K. Shayan, S. Strauf, J. L. Blackburn, S. Tretiak, S. K. Doorn and H. Htoon, *ACS Nano*, 2017, **11**, 10785–10796.
- 21 Y. Maeda, K. Kuroda, H. Tambo, H. Murakoshi, Y. Konno, M. Yamada, P. Zhao, X. Zhao, S. Nagase and M. Ehara, *RSC Adv.*, 2019, **9**, 13998–14003.
- 22 A. B. I. Smith, R. M. Strongin, L. Brard, G. T. Furst, W. J. Romanow, K. G. O'wens, R. J. Goldschmidt and R. C. King, *J. Am. Chem. Soc.*, 1995, **117**, 5492–5502.
- 23 M. Eiermann, F. Wudl, M. Prato and M. Maggini, *J. Am. Chem. Soc.*, 1994, **116**, 8364–8365.
- 24 R. A. J. Jassen, J. C. Hummelen and F. Wudl, *J. Am. Chem. Soc.*, 1995, **117**, 544–545.
- 25 W.-W. Yang, Z.-J. Li, F.-F. Li and X. Gao, *J. Org. Chem.*, 2011, **76**, 1384–1389.
- 26 E. Allard, L. Rivière, J. Delaunay, D. Dubois and J. Cousseau, *Tetrahedron Lett.*, 1999, **40**, 7223–7226.
- 27 Y. Maeda, Y. Takehana, J. S. Dang, M. Suzuki, M. Yamada and S. Nagase, *Chem. – Eur. J.*, 2017, **23**, 1789–1794.
- 28 A. D. Becke and C. H. Schiesser, *Tetrahedron Lett.*, 1985, **41**, 3925–3941.
- 29 C. Lee, W. Yang and R. G. Parr, *Phys. Rev. B: Condens. Matter Mater. Phys.*, 1988, **37**, 785–789.
- 30 M. J. Frisch, G. W. Trucks, H. B. Schlegel, G. E. Scuseria, M. A. Robb, J. R. Cheeseman, G. Scalmani, V. Barone, B. Mennucci and G. A. Petersson, *et al.*, *Gaussian 09, Revision E.01*, Gaussian, Inc., Wallingford CT, 2013.
- 31 A. D. Becke, *J. Chem. Phys.*, 1993, **98**, 5648–5652.
- 32 T. Yanai and D. P. Tew, *Chem. Phys. Lett.*, 2004, **393**, 51–57.
- 33 Y. Maeda, Y. Konno, M. Yamada, P. Zhao, X. Zhao, M. Ehara and S. Nagase, *Nanoscale*, 2018, **10**, 23012–23017.
- 34 B. J. Gifford, A. E. Sifain, H. Htoon, S. K. Doorn, S. Kilina and S. Tretiak, *J. Phys. Chem. Lett.*, 2018, **9**, 2460–2468.